DOCTORAL THESIS

Distinguishing true from pseudo hematoma in the cervical spinal canal using postmortem computed tomography

（死後 CT 画像を用いた真と疑似の頸椎脊柱管内血腫の鑑別）

March, 2024

（2024 年 3 月）

Hikaru Kuninaka

國中　光

Legal Medicine,

Yokohama City University Graduate School of Medicine

横浜市立大学　大学院医学研究科　医科学専攻　法医学

(Doctoral Supervisor：Yoko Ihama, Professor)

（指導教員：井濱容子教授）

Legal Medicine 66 (2024) 102358

Contents lists available at ScienceDirect

Legal Medicine

journal homepage: www.elsevier.com/locate/legalmed

Distinguishing true from pseudo hematoma in the cervical spinal canal using postmortem computed tomography

Hikaru Kuninaka [a], Yosuke Usumoto [a,b], Momoka Tanabe [a], Noriko Ogawa [a], Moe Mukai [a], Ayako Nasu [a], Kazuho Maeda [a], Chiaki Fuke [a], Shungo Sawamura [c], Tsuneo Yamashiro [c], Daisuke Utsunomiya [c], Yoko Ihama [a,*]

[a] Department of Legal Medicine, Yokohama City University Graduate School of Medicine, 3-9 Fukuura, Kanazawa, Yokohama, Kanagawa 236-0004, Japan
[b] Department of Forensic Pathology and Sciences, Graduate School of Medical Sciences, Kyushu University, 3-1-1 Maidashi, Higashi, Fukuoka, Fukuoka 812-8582, Japan
[c] Department of Diagnostic Radiology, Yokohama City University Graduate School of Medicine, 3-9 Fukuura, Kanazawa, Yokohama, Kanagawa 236-0004, Japan

ARTICLE INFO

Keywords:
Pseudo hematoma in the cervical spinal canal
Postmortem computed tomography
Spinal cord injury
Forensic autopsy
Internal vertebral venous plexus
Forensic imaging

ABSTRACT

Spinal cord injury is difficult to detect directly on postmortem computed tomography (PMCT) and it is usually diagnosed by indirect findings such as a hematoma in the spinal canal. However, we have encountered cases where the hematoma-like high-attenuation area in the cervical spinal canal was visible on PMCT, while no hematoma was observed at autopsy; we called it a "pseudo hematoma in the cervical spinal canal (pseudo-HCSC)." In this retrospective study, we performed statistical analysis to distinguish true from pseudo-HCSC. The cervical spinal canal was dissected in 35 autopsy cases with a hematoma-like high-attenuation area (CT values 60–100 Hounsfield Unit (HU)) in the spinal canal from the first to the fourth cervical vertebrae in axial slices of PMCT images. Of these 22 had a hematoma and 13 did not (pseudo-HCSC). The location and length of the hematoma-like high-attenuation and spinal cord areas were assessed on reconstructed PMCT images, true HCSC cases had longer the posterior hematoma-like area and shorter the spinal cord area in the midline of the spinal canal ($P < 0.05$). Furthermore, we found that true HCSC cases were more likely to have fractures and gases on PMCT while pseudo-HCSC cases were more likely to have significant facial congestion ($P < 0.05$). We suggest that pseudo-HCSC on PMCT is related to congestion of the internal vertebral venous plexus. This study raises awareness about the importance of distinguishing true HCSC from pseudo-HCSC in PMCT diagnosis, and it also presents methods for differentiation between these two groups.

1. Introduction

Upper cervical spinal cord injury is associated with a high mortality rate of 48.3–79.0% and can cause paralysis of the respiratory muscles and neurogenic shock as a direct cause of death [1,2]. In addition, it can cause drowning or infections related to paralysis as indirect causes of death [1,3,4]. An accurate diagnosis of cervical cord injury is important to determine the cause of death in forensic medicine, but it is difficult to detect a spinal cord injury directly on postmortem computed tomography (PMCT) images. Therefore, several previous studies have attempted to diagnose cervical spinal cord injuries based on cervical spine fractures and spinal ligament injuries using PMCT images [2,5–9].

Clinically, a hematoma-like high-attenuation area in the spinal canal on CT images is used as a diagnostic factor of hematoma [10,11]; while few studies have reported that it can be used as a similar factor in forensic medicine. Therefore, in our preliminary analysis we compared PMCT images and autopsy findings, focusing on a hematoma-like high-attenuation area in the cervical spinal canal on PMCT image. In one case, a hematoma-like high attenuation area in the cervical spinal canal was visible on PMCT images, and spinal epidural hematoma (SEDH) was found at autopsy (Fig. 1A, B). However, in another case, a hematoma-like high-attenuation area in the cervical spinal canal was visible on

* Corresponding author.
E-mail addresses: t206026c@yokohama-cu.ac.jp (H. Kuninaka), usumoto.yosuke.927@m.kyushu-u.ac.jp (Y. Usumoto), tanabe.mom.aq@yokohama-cu.ac.jp (M. Tanabe), mukai@yokohama-cu.ac.jp (M. Mukai), aykns@yokohama-cu.ac.jp (A. Nasu), maedak@yokohama-cu.ac.jp (K. Maeda), cfuke@yokohama-cu.ac.jp (C. Fuke), sawa0808@yokohama-cu.ac.jp (S. Sawamura), clatsune@yahoo.co.jp (T. Yamashiro), d_utsuno@yokohama-cu.ac.jp (D. Utsunomiya), ihama@yokohama-cu.ac.jp (Y. Ihama).

https://doi.org/10.1016/j.legalmed.2023.102358
Received 3 August 2023; Received in revised form 14 November 2023; Accepted 16 November 2023
Available online 29 November 2023

PMCT images, while no hematoma was found at autopsy (Fig. 1C, D). This means that attempting to diagnose hematoma based solely on the presence of hematoma-like high-attenuation areas on PMCT may lead to misdiagnosis. To avoid such misdiagnosis, we coined a novel term "pseudo cervical spinal canal hematoma (pseudo-HCSC)" to describe a hematoma-like high-attenuation area in the cervical spinal canal on PMCT image when there was no real hematoma. In this study, we aimed to establish a method for accurately distinguish true from pseudo-HCSC using PMCT images and autopsy findings.

2. Materials and methods

2.1. Study group

We retrospectively reviewed the data of 499 forensic autopsy cases in which PMCT scans were performed at our institution from December 2018 to June 2022. We excluded cases of individuals under 18 years of age or cases that could not be properly evaluated on PMCT images, such as those involving cerebral softening, residual contrast agent, and significant cervical deviation. The remaining 338 cases were used for screening tests. Positive screening cases were those with a hematoma-like high-attenuation area (CT values 60–100 Hounsfield Unit (HU)) in the spinal canal from the first to the fourth cervical vertebrae (C1-4) in axial slices of PMCT images. We set the CT values of hematoma-like high attenuation between 60 and 100 HU because previous reports indicated that the CT values of hematomas were higher postmortem than antemortem [12–14]. There were 140 positive cases, of which 35 underwent cervical spine dissection and were included in the measurement group. The measurement group data on the age, sex, cause of death, autopsy findings of the cervical spinal cord, height, weight, postmortem interval between death and PMCT scan (PMI-CT), and PMI between death and autopsy (PMI-autopsy) of the deceased were collected.

2.2. CT technique

PMCT scans were performed before autopsy using a 16-row multidetector CT scanner (Aquilion Lightning; Canon Medical Systems, Otawara, Tochigi, Japan). Twenty-four cases were performed autopsy after the PMCT scan, and in 11 cases, the bodies were stored at 4 °C in a morgue until autopsy. All bodies were placed in a body bag in a supine position without elevation of the upper limbs and scanned from the head to the pelvis. No contrast agents were used. Only head CT was used in the study with the following parameters: detector collimation, 16 × 1 mm (helical scanning); gantry rotation time, 0.5 sec; beam pitch, 0.94; tube voltage, 120 kVp; tube current, 130–230 mA (auto exposure control). The PMCT images were reconstructed with 1-mm slice thickness and 1-mm interval, and sent to a workstation (Synapse Vincent; Fujifilm Medical, Tokyo, Japan) for further image analysis.

2.3. Autopsy

Two board-certified forensic pathologists (YI and YU) performed all the autopsies to determine the cause of death. postmortem lividity and facial congestion were assessed at external examination. Cases with severe and moderate postmortem lividity were rated +, and otherwise were rated -. Cases with significant facial congestion were rated +, and otherwise were rated -. However, postmortem lividity and facial hyperemia were not evaluated if they could not be observed from the body surface due to burn. Additionally, the volume of cardiac blood was measured when the heart was removed. Then the presence of intracranial hemorrhage was assessed. To dissect the cervical vertebrae in the measurement group, the cervical spinal cord was removed from the anterior or posterior side and observed circumferentially. The cases that had hematomas in the C1-4 spinal canals at autopsy were designated as "true HCSC" and those that had no hematoma were classified as "pseudo-HCSC." Histopathological examination was not performed in this study.

2.4. PMCT image evaluation procedure

For the measurement group, we reconstructed C1-4 such that the PMCT images matched the height and position of the spinal canal in the axial slice of each case. First, multi-planar reconstruction (MPR) images were acquired by processing the PMCT images using a CT workstation, and the bone window setting (window width (WW)/window level (WL), 1500/450 HU) was displayed (Supplementary Fig. 1). Regarding C1-4, the left and right transverse processes were adjusted to appear symmetrical in the coronal slice, and the line connecting the left and right transverse processes was aligned directly with the midline of the vertebral body (Supplementary Fig. 1A). For C1, we obtained an axial slice from the line connecting the anterior and posterior tuberosities, passing through the point where the widths of the left and right posterior arches were the narrowest in the sagittal slice. For C2, an axial slice was obtained from the sagittal slice through the point where the widths of the left and right vertebral arches narrowed down(Supplementary Fig. 1B) and were horizontal to the lower vertebral body

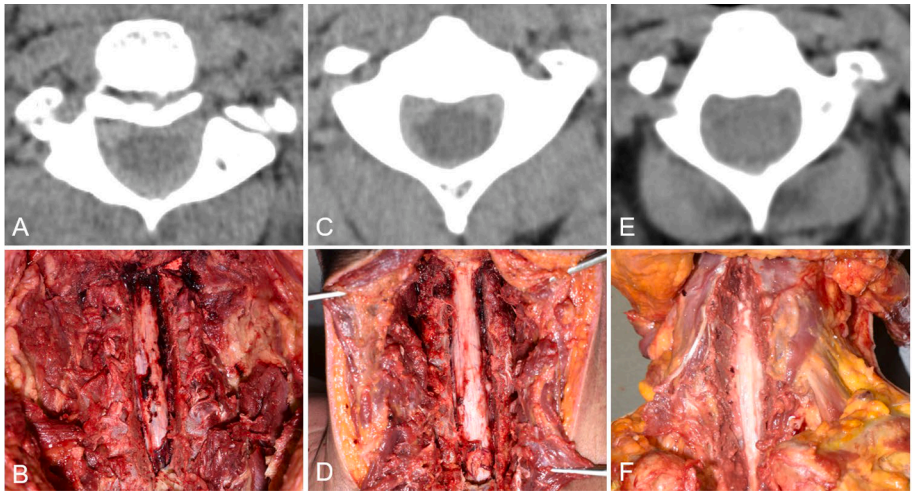

Fig. 1. Postmortem computed tomography (PMCT) images of the axial slice on the second cervical vertebra (WW/WL, 300/40 HU) and autopsy findings of three cases. A, B: PMCT image and autopsy findings of a cervical spinal cord injury case. C, D: PMCT image and autopsy findings of an acute myocardial infarction case. E, F: PMCT image showing no hematoma-like high attenuation area in the cervical spinal canal and autopsy findings showing no hematoma, of a hemothorax case.

(Supplementary Fig. 1C, D). For C3 and C4, axial slices were obtained from the sagittal slice through the narrowest point of the left and right vertebral arches horizontal to the upper vertebral body.

Furthermore, the lengths of each axial slice (C1-4) obtained using the above procedure were measured as follows: first, the soft tissue window setting (WW/WL, 300/40 HU) of the axial slice was displayed. Then, the areas in the spinal canal with CT values of 60–100 HU were displayed in yellow, and the midline of the spinal canal was drawn (Fig. 2). Next, from the anterior to the posterior side, five lengths were identified as follows: the gray area, consisting of the periosteum and ligaments ((a), (e)); the yellow area, involving CT values of 60–100 HU ((b), (d)); and the dark gray area, consisting of the spinal cord and cerebrospinal fluid (CSF) (c). The spinal canal anteroposterior (AP) diameter was determined by summing the measurements from (a), (b), (c), (d), and (e). The reconstructed cervical vertebrae (C1-4) in which accurate measurements were not possible due to artifacts or cervical spine fractures were not evaluated, and only the sites that could be measured were considered. Moreover, the area of the region with CT values of 60–100 HU within the spinal canal (area of 60–100 HU) and the mean CT values were measured. Area of 60–100 HU was not evaluated for C1 because of the complex shape of the spinal canal.

To estimate the intra-observer measurement error, all cases in the measurement group were re-evaluated at least 1 month after the initial evaluation. To estimate the inter-observer measurement error, the images were measured twice by different forensic pathologists (HK and YU) at least 1 month apart. In the measurement group, all cervical spine fractures and cervical spinal canal gases were evaluated using the MPR images.

2.5. Statistical analysis

Data were analyzed using the JMP 16.0 Pro (SAS Institute Inc., Cary, North Carolina, USA). Welch's *t*-test was used to compare between the true HCSC group and pseudo-HCSC group regarding height, weight, body mass index (BMI), PMI-CT, cardiac blood volume, each measured length ((a)-(e)), spinal canal AP diameter, measured length/spinal canal AP diameter, area of 60–100 HU, and mean CT values. We also compared between the two groups using Fisher's exact probability test for sex, postmortem lividity, facial congestion, intracranial hemorrhage, cervical spine fractures, and cervical spinal canal gases on PMCT images. Statistical significance was set at $P < 0.05$.

Subsequently, equations predicting the true HCSC groups at each cervical spine were developed using multiple logistic regression analyses. A maximum of three variables were selected by combining all the items examined (age, sex, height, weight, BMI, PMI-CT, postmortem lividity, facial congestion, cardiac blood volume, intracranial injury, cervical spine fractures on PMCT images, cervical spinal canal gases on PMCT images, each length measured on the reconstructed PMCT image, length measured/spinal canal AP diameter, area of 60–100 HU, and mean CT value). The best combination of variables was determined based on the smallest Akaike's information criterion corrected for small sample sizes (AICc) [15,16]. Cases in which a unique formula could not be determined using the variable combination were excluded. The variance inflation factor (VIF) was calculated to assess multicollinearity among the variables. The VIF evaluation criteria were defined as failed: >10, poor: ≥ 5, and good: < 5 [17,18]. In addition, variables with values below 5 were retained. Furthermore, the receiver operating characteristic (ROC) curve analysis was used to calculate the area under the curve (AUC) to evaluate the discriminative ability of each formula. The AUC results were defined as failed: 0.5–0.6, poor: 0.6–0.7, fair: 0.7–0.8, good: 0.8–0.9, and excellent: 0.9–1 [19–21].

We used R version 4.2.2 (R Foundation for Statistical Computing, Vienna, Austria) to calculate the technical error of measurement (TEM), relative technical error of measurement (rTEM), and coefficient of reliability (R) for both intra-observer and inter-observer errors within the measurement group. The evaluation criteria for rTEM, which are generally used for anthropometry in anthropology, defined an intra-observer rTEM $< 1.5\%$ and an inter-observer rTEM $< 2.0\%$ as extremely small errors [22]. The R value was evaluated by defining R greater than 0.95 as high reliability [23].

2.6. Ethics

This study was approved by Yokohama City University Ethics Committee (F230202313). Informed consent from the bereaved families was not required because the study used existing specimens without invasion or intervention.

3. Results

3.1. Autopsy results of the measurement group

Of the 35 cases in the measurement group, 22 were ultimately diagnosed with hematoma at autopsy were classified into the true HCSC group (SEDH, 14; combinations of SEDH, spinal subdural hematoma (SSDH) and spinal subarachnoid hematoma (SSAH), 5; combinations of SSDH and SSAH, 3). Thirteen cases without hematomas at autopsy were classified into the pseudo-HCSC group (Supplementary Table 1).

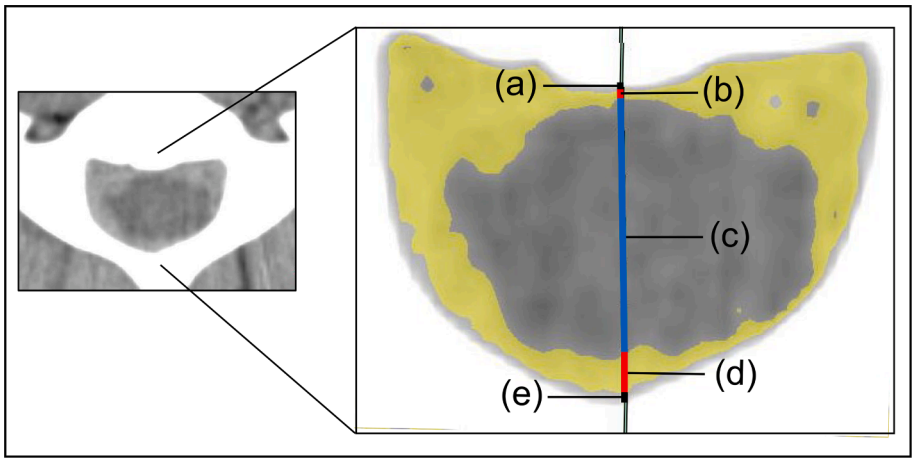

Fig. 2. Reconstructed axial slice on the second cervical vertebra and magnified spinal canal with midline measurements (WW/WL, 300/40 HU). (a): anterior length of the periosteum and ligaments. (b): anterior length of the yellow area with CT values of 60–100 HU, (c): length of the spinal cord and cerebrospinal fluid area. (d): posterior length of the yellow area with CT values of 60–100 HU. (e): posterior length of the periosteum and ligaments.

The measurement group comprised 21 males and 14 females with a mean age of 60.7 years. The true HCSC group comprised 14 males and 8 females with a mean age of 61.8 years, and the pseudo-HCSC group comprised 7 males and 6 females with a mean age of 59.0 years. There were no statistically significant differences in age ($P = 0.72$), sex ($P = 0.72$), height ($P = 0.62$), weight ($P = 0.92$), BMI ($P = 0.91$), or PMI-CT ($P = 0.27$) between the two groups (Table 1). Moreover, there were no statistically significant differences between the two groups regarding-postmortem lividity ($P = 0.066$), cardiac blood volume ($P = 0.074$), and intracranial hemorrhage ($P = 0.086$) (Table 2, Supplementary Fig. 2). However, more facial congestions were observed in the pseudo-HCSC group ($P = 0.00091$; one case in the pseudo-HCSC group could not be determined due to burn) (Table 2, Supplementary Table 1).

3.2. Intra- and Inter-Observer errors

The intra-observer rTEM ranged from 0.82 to 52.16%, and the R values ranged from 0.9414 to 0.9978 (Supplementary Table 2). The inter-observer rTEM ranged from 0.99 to 61.02%, and the R values ranged from 0.6277 to 0.9999. Few variables had intra-observer rTEM $< 1.5\%$ and inter-observer rTEM $< 2.0\%$; however, for (c), the intra- and inter-observer rTEM tended to be smaller than the other variables at any cervical height. The intra- and inter-observer R values were below 0.95 for some items, but for (c), they were above 0.95 for all cervical heights.

3.3. Results of the measurements regarding the PMCT images in 35 cases in the measurement group

Of the 35 cases in the measurement group, 26 cases (true HCSC, 16; pseudo-HCSC, 10) were measured in the reconstructed cervical vertebrae in C1, 18 cases (true HCSC, 10; pseudo-HCSC, 8) in C2, 31 cases (true HCSC, 19; pseudo-HCSC, 12) in C3, and 26 cases (true HCSC, 14; pseudo-HCSC, 12) in C4 (Supplementary Table 3). Other sites could not be evaluated because of artifacts or fractures.

At each cervical spine height, the length of (a) between (e), (a) + (b) + (c) + (d) + (e) (spinal canal AP diameter), (b) + (d) (total length of the yellow area with CT values of 60–100 HU), measured length/spinal canal AP diameter, area of 60–100 HU, and the mean CT value were compared between the two groups (Supplementary Table 4). There was no statistically significant difference between the two groups regarding the length of (a), length of (b), (b)/spinal canal AP diameter, length of (e), and length of spinal canal AP diameter (Fig. 3A, B, E, G, K). Moreover, there was no statistically significant difference between the two groups regarding area of 60–100 HU and the mean CT value (Fig. 3L, M).

There was no significant difference in the length of (c) between the two groups (Fig. 3C); however, (c)/spinal canal AP diameter was significantly larger in the pseudo-HCSC group at all heights except C1 (Fig. 3H). In the true HCSC group, the length of (d) and (d)/spinal canal AP diameter were significantly longer and larger at all cervical spine heights (Fig. 3D, I). Moreover, in the true HCSC group, the length of (b) + (d) and ((b) + (d))/spinal canal AP diameter were significantly longer and larger than those in the pseudo-HCSC group at all heights except for C1 (Fig. 3F, J).

Regarding cervical spine fractures on PMCT images, the true HCSC group had a significantly higher incidence rate ($P = 0.0039$), as did cervical spinal canal gases on PMCT images ($P = 0.0052$) (Table 2).

Table 1
Measurement group profile.

Variable		True HCSC (n = 22) Mean (Range)	n	Pseudo-HCSC (n = 13) Mean (Range)	n	*P* value
age [year]		61.8 (22–93)		59.0 (34–86)		0.72
sex	M		14		7	0.72
	F		8		6	
height [cm]		164.5 (142–180)		162.7 (144–179)		0.62
weight [kg]		61.8 (28.7–119.2)		61.1 (36–93.4)		0.92
BMI		22.4 (11.9–37.2)		22.6 (16.8–30.8)		0.91
PMI-CT [h]		86.5 (17–240)		66.9 (9–160)		0.27
PMI-autopsy [h]		93.6 (17–240)		78.8 (29–160)		0.40

HCSC: hematoma in the cervical spinal canal; PMI: postmortem interval.

Table 2
Details regarding the findings of the autopsy and postmortem computed tomography images.

	Postmortem lividity		Facial congestion		Intracranial hemorrhage		Cervical fractures on PMCT		Cervical spinal canal gases on PMCT	
	+	−	+	−	+	−	+	−	+	−
True HCSC	10	12	2	20	14	8	13	9	10	12
Pseudo-HCSC	10	2	8	4	4	9	1	12	0	13
P value	0.066		0.00091*		0.086		0.0039*		0.0052*	

Postmortem lvidity and facial congestion could not be determined in one case in the pseudo-HCHC group due to burn.
*: $P < 0.05$.

3.4. Results of the multiple logistic regression analysis

The multiple logistic regression analysis was used to develop equations for predicting outcomes in the true HCSC group (Table 3). The measurement factors were not adopted in the equation with the minimum AICc at the height of C3, and only one factor, facial congestion, was adopted. At any cervical height, the ROC curve analysis showed that the AUC exceeded 0.7–0.8.

4. Discussion

Autopsy is considered the most reliable method for determining the cause of death; however, the autopsy rate in Japan is lower than that in other countries, and greatly differs among regions [24]. Hence, postmortem imaging, which involves CT or magnetic resonance imaging of cadavers, is expected to play an active role as an alternative to autopsy or as an auxiliary tool for determining the cause of death [25,26]. The PMCT is one of the most popular diagnostic imaging modalities used in Japan [27]. However, PMCT images are influenced by postmortem changes, and many findings differ from those of antemortem CT images [28]. Some of these changes are usually caused by modifications of the body due to medical treatments, resuscitation, and other changes, such as hypostasis and generation of decomposition gases. Not knowing these factors may lead to underestimation or overestimation of findings and lesions on PMCT images. Especially because not all of these postmortem changes are fully understood and PMCT is still a developing diagnostic tool. Therefore, it is necessary to improve the diagnostic accuracy of PMCT by comparing it with autopsy findings and antemortem CT.

In forensic autopsy, we do not always dissect the spinal canal in all cases; the examination for directly observing the spinal cord removed from the spinal canal is limited to cases where spinal cord injury is strongly suspected based on circumstances in which the body was found and/or external findings. On PMCT image, hematoma-like high attenuation area in the cervical spinal canal is an important finding that helps suspect cervical spinal cord injury [29]. Nevertheless, in this study, no hematomas were observed in 13 (37.1%) of the 35 cases in the measurement group. This means that diagnosing HCSC only from PMCT images without checking the spinal canal at autopsy may lead to

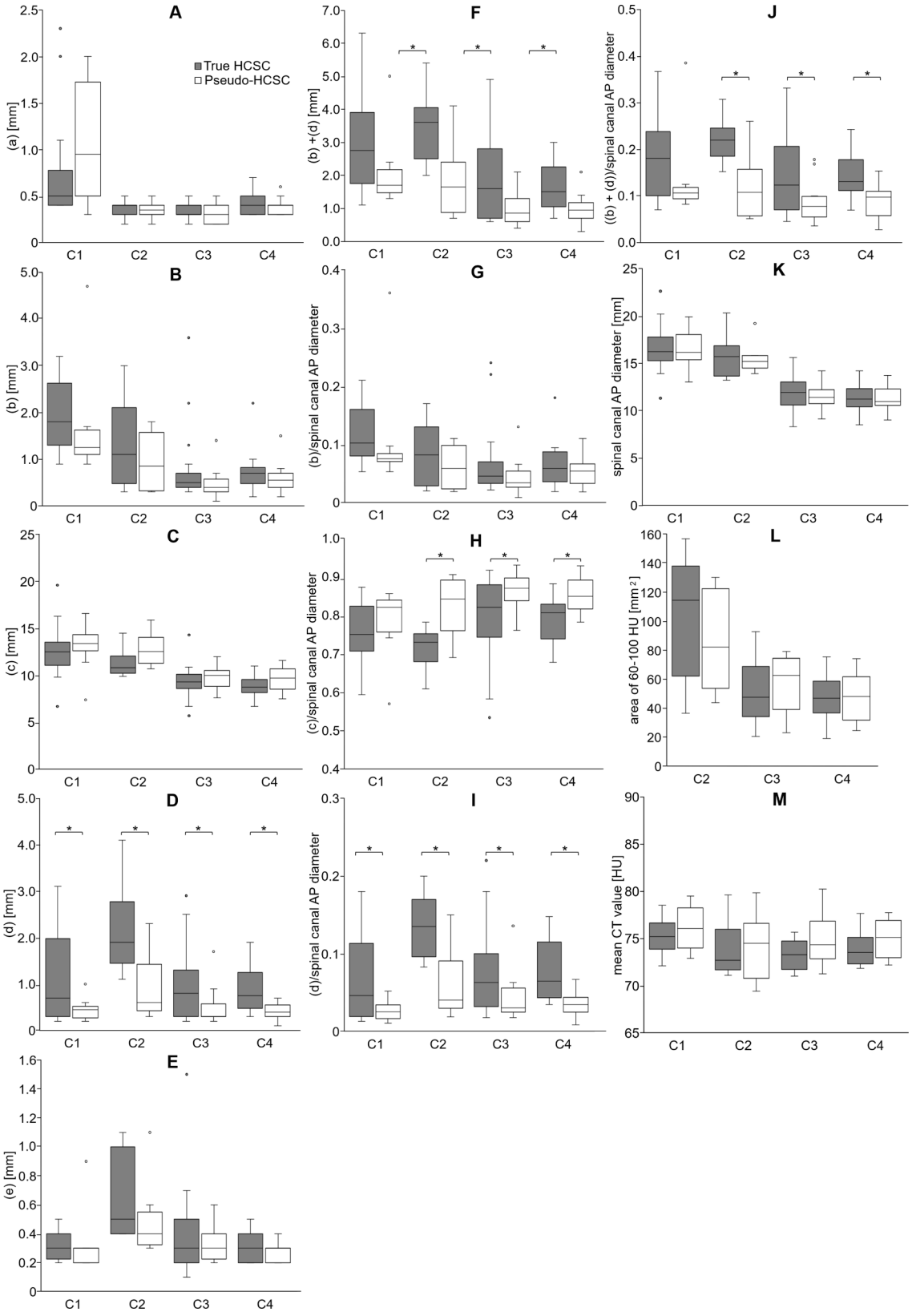

Fig. 3. Measurements of the true and pseudo hematoma in the cervical spinal canal (HCSC) groups at each cervical spine height. In a box plot, the horizontal line inside the box represents the median, the bottom end of the box represents the first quartile (25%), the top of the box represents the third quartile (75%), the whiskers extend up to a maximum and minimum value that is within 1.5 times the length of the box, and the plots represent outlier data outside 1.5 times. A: Length of (a). B: Length of (b). C: Length of (c). D: Length of (d). E: Length of (e). F: Length of (b) + (d). G: (b)/spinal canal AP diameter. H: (c)/spinal canal AP diameter. I: (d)/spinal canal AP diameter. J: ((b) + (d))/spinal canal AP diameter. K: Length of spinal canal anteroposterior (AP) diameter. L: The area of the region with CT values of 60–100 HU within the spinal canal (area of 60–100 HU). M: mean CT value. *: $P < 0.05$.

Table 3
Results of the multiple logistic regression analysis at each cervical height.

	Coefficient	SE	Wald χ^2	*P* value	Odds ratio	95% CI	AICc	AUC
C1							27.66	0.88
Intercept	−2.93	1.91	–	0.13	–	–		
Facial congestion	1.00	0.55	3.29	0.07	0.13	0.02 to 1.18		
Length of (b) + (d)	1.55	0.98	2.50	0.11	4.69	0.69 to 31.80		
C2							14.98	0.97
Intercept	31.05	17.20	–	0.07	–	–		
Facial congestion	2.57	1.44	3.17	0.07	5.85×10^{-3}	2.05×10^{-5} to 1.67		
(c)/spinal canal AP diameter	−40.51	22.39	3.27	0.07	2.55×10^{-18}	2.24×10^{-37} to 29.04		
C3							34.43	0.77
Intercept	0.10	0.49	–	0.84	–	–		
Facial congestion	1.35	0.49	7.66	0.01	0.07	0.01 to 0.45		
C4							21.75	0.93
Intercept	−8.28	5.26	–	0.12	–	–		
Facial congestion	2.58	1.50	2.95	0.09	5.72×10^{-3}	1.58×10^{-5} to 2.07		
Length of (d)	14.78	9.84	2.26	0.13	2.63×10^{6}	0.01 to 6.23×10^{14}		

AP: anteroposterior; SE: standard error; CI: confidence interval; AICc: Akaike's information criterion corrected for small sample sizes; AUC: area under the curve.

misdiagnosis of the cause of death. To date, no study has reported a pseudo-HCSC. Accordingly, we suggest that caution should be taken when diagnosing a hematoma around the cervical cord using PMCT.

Although the factors that cause pseudo-HCSC are not clear, we hypothesize that epidural vascular congestion might appear as a hematoma on PMCT. In the pseudo-HCSC group, the epidural vessels were often congested when the spinal canal was opened. Anatomically, the internal vertebral venous plexus (IVVP) develops in the epidural space within the spinal canal (Fig. 4) [30,31]. The IVVP consists of the anterior and posterior IVVP and forms a vascular ring around the spinal dura mater from the cranial vault to the sacrum. The IVVP has been reported to have no valve structure, blood is occasionally congested [32,33]. Several articles have reported pseudo subarachnoid hematoma (pseudo-SAH), in which intracranial SAH was seen on PMCT images but not at autopsy [34–36]. Takahashi et al. reported that increased attenuation of the transverse sinus or cerebellar tentorium on PMCT images was observed in 48% including autopsy cases. They suggest that blood congestion in the dural venous sinuses included in the cranial venous system, such as the superior sagittal and transverse venous sinuses, and the settling and further concentration of the cellular components of the blood by gravity are the causes of hematoma-like high-attenuation areas on PMCT images [35]. Anatomically, the cranial venous system and vertebral venous plexus including the IVVP form a common venous network called the cerebrospinal venous system (CSVS) [30]. We believe that pseudo-HCSC may have the same underlying cause as pseudo-SAH, that is, blood congestion in the CSVS. Techniques such as PMCT angiography and postmortem magnetic resonance imaging may help prove our hypothesis in the future.

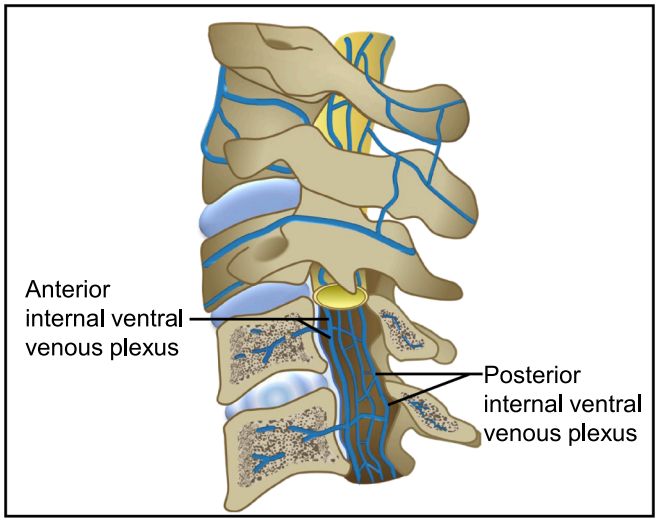

Fig. 4. Schematic view of the internal vertebral venous plexus and its components.

Using multiple logistic regression analysis, we could discriminate between the true and pseudo-HCSC groups based on the measurement results and collected data. The ROC curve analysis for the equations developed at each cervical spine height showed that the discriminatory ability was sufficient, as all AUCs exceeded 0.7. The highest AUC was 0.97 at the height of C2 (Table 3). Despite this, only half of the cases could be measured (18/35) in C2 due to artifacts from intraoral metals and medical devices. Practically, based on the fact that many cases could be measured (26/35) and had a high AUC of 0.93, the height of C4 was the most suitable for differentiation (Table 3; Supplementary Table 3).

In addition, the results of the multiple logistic regression analysis showed that "facial congestion" was the most useful factor for differentiating two groups (Table 3). The pseudo-HCSC group had more cases with facial congestion than the true HCSC group (Table 2). In the pseudo-HCSC group, 8 of the 13 cases had facial congestion, many of the causes of death were generally those considered likely to cause head congestion (Supplementary Table 1). Congestion in the head and neck region brings the congestion of IVVP, and they could cause a pseudo-HCSC. If a case with significant face congestion shows a hematoma-like high-attenuation area in the cervical spinal canal on PMCT, a pseudo-HCSC should be suspected. On the other hand, the cause of death in 3 of the 4 pseudo-HCSC cases without facial congestion was hypoxic-ischemic encephalopathy (Supplementary Table 1). Several studies have reported that pseudo-SAH on PMCT images arise in cases with diffuse cerebral edema [36–38]. Shirota et al. reported that the putative mechanism underlying pseudo-SAH on PMCT images was a disturbance of venous drainage caused by swelling of the brain, which led to congestion of the subarachnoid and parenchymal blood vessels [36]. Similarly, the disturbance of venous drainage within the cervical spinal canal may cause pseudo-HCSC.

In addition to facial congestion, based on the results of the multiple logistic regression analysis, some of the measurements in the PMCT images were useful in predicting true HCSC (Table 3). The length of (d), i.e., the posterior length of the yellow area with CT values of 60–100 HU was significantly greater in the true HCSC group than in the pseudo-HCSC group (Fig. 3D). From this result, it is reasonable to consider that the hematoma-like high attenuation area in the cervical spinal canal is an extravascular hematoma in true HCSC and a congestion of the IVVP in pseudo-HCSC. Indeed, in the true HCSC group, 12 SEDH cases of

which had a posterior hematoma (Supplementary Table 1). Furthermore, clinically, many studies have reported that SEDH is more common posterior side [39,40], consistent with the location of this study results. The length of (c) is the midline of the spinal cord and the CSF. When the length of (c) is long, the length of (b)+(d)) decreases, and when the length of (c) is short, the length of ((b)+(d)) increases (Fig. 2, Fig. 3C, F, H, J). Hence, (c) and (b) + (d) are inversely related. The (c)/spinal canal AP diameter was significantly smaller in the true HCSC group than in the pseudo-HCSC group (Fig. 3H), and this result shows compression of the spinal cord by hematoma. Clinically, there are several reports of spinal cord compression due to hematoma [40,41], which supports the fact that (c) was shortened by the hematoma ((b) + (d)) in the true HCSC group.

Many of the factors measured in this study had an rTEM greater than 1.5% or 2.0% and R<0.95 (Supplementary Table 2). This may have been due to the complexity of the procedure used to reconstruct the PMCT images so that the height and position of the spinal canal in the axial slice of each case matched. In addition, technical errors due to manual manipulation may have greatly affected the measured values because they were extremely small. The measurement method used in this study is a new method that has not been used in previous studies. Furthermore, the measured value of (c) was larger than those of (a), (b), (d), and (e); the rTEM of the error was smaller, and R was greater than 0.95. Consequently, (c) was associated with a small error and high reliability in this study.

Incidentally, cervical spinal canal gases on PMCT images are extremely useful as a factor to suspect true HCSC, as none was observed in the pseudo-HCSC group in this study (Table 2). There was also a statistically significant difference between the two groups regarding cervical spine fractures on PMCT images; cervical spine fractures were more common in the true HCSC group (Table 2). Gases and cervical spine fractures which serves evidence of strong external force applied to the neck, are important findings suggestive of true HCSC.

This study has limitations. The number of cases included in this study was small, and the statistical analysis was insufficient. In the future, we intend to increase the number of cases to improve the accurate diagnose using PMCT for hematoma in the spinal canal.

5. Conclusion

In this study, we showed the presence of a pseudo-HCSC, and suggest that pseudo-HCSC are related to the congestion of the IVVP and disturbance of venous drainage. We performed statistical analysis to distinguish between true and pseudo-HCSC on PMCT. True HCSC cases had longer the posterior hematoma-like area and shorter the spinal cord area in the midline of the spinal canal ($P < 0.05$). Furthermore, we found that true HCSC cases were more likely to have fractures and gases on PMCT and pseudo-HCSC cases were more likely to have significant facial congestion ($P < 0.05$). These factors were found to be useful in distinguishing between the two groups.

Declaration of Competing Interest

The authors declare that they have no known competing financial interests or personal relationships that could have appeared to influence the work reported in this paper.

Appendix A. Supplementary material

Supplementary data to this article can be found online at https://doi.org/10.1016/j.legalmed.2023.102358.

References

[1] L.H. Sekhon, M.G. Fehlings, Epidemiology, demographics, and pathophysiology of acute spinal cord injury, Spine (Phila Pa 1976) 26 (2001) S2–S12, https://doi.org/10.1097/00007632-200112151-00002.

[2] H. Iwase, S. Yamamoto, D. Yajima, M. Hayakawa, K. Kobayashi, K. Otsuka, K. Sato, H. Motani, S. Kasahara, H. Ito, Can cervical spine injury be correctly diagnosed by postmortem computed tomography? Leg. Med. 11 (2009) 168–174, https://doi.org/10.1016/j.legalmed.2009.02.032.

[3] R.J. Soden, J. Walsh, J.W. Middleton, M.L. Craven, S.B. Rutkowski, J.D. Yeo, Causes of death after spinal cord injury, Spinal Cord. 38 (10) (2000) 604–610, https://doi.org/10.1038/sj.sc.3101080.

[4] I.G. Malone, R.L. Nosacka, M.A. Nash, K.J. Otto, E.A. Dale, Electrical epidural stimulation of the cervical spinal cord: implications for spinal respiratory neuroplasticity after spinal cord injury, J. Neurophysiol. 126 (2) (2021) 607–626, https://doi.org/10.1152/jn.00625.2020.

[5] Y. Makino, H. Yokota, E. Nakatani, D. Yajima, G. Inoguchi, A. Motomura, F. Chiba, S. Torimitsu, T. Uno, H. Iwase, Differences between postmortem CT and autopsy in death investigation of cervical spine injuries, Forensic Sci. Int. 281 (2017) 44–51, https://doi.org/10.1016/j.forsciint.2017.10.029.

[6] K. Yen, M. Sonnenschein, M.J. Thali, C. Ozdoba, J. Weis, K. Zwygart, E. Aghayev, C. Jackowski, R. Dirnhofer, Postmortem multislice computed tomography and magnetic resonance imaging of odontoid fractures, atlantoaxial distractions and ascending medullary edema, Int. J. Legal Med. 119 (3) (2005) 129–136, https://doi.org/10.1007/s00414-004-0507-7.

[7] T. Okuda, S. Shiotani, H. Hayakawa, K. Kikuchi, T. Kobayashi, Y. Ohno, A case of fatal cervical discoligamentous hyperextension injury without fracture: correlation of postmortem imaging and autopsy findings, Forensic Sci. Int. 225 (1–3) (2013) 71–74, https://doi.org/10.1016/j.forsciint.2012.04.035.

[8] S. Kudo, Y. Kawasumi, A. Usui, M. Arakawa. N. Yamagishi, Y. Igari, M. Funayama, T. Ishibashi, Post-mortem computed tomography of cervical intervertebral separation: Retrospective review and comparison of the autopsy results of 57 separations, J. Forensic Radiol. Imaging 12(2018) 57-63. 10.1016/J.JOFRI.2018.02.007.

[9] S. Kudo, Y. Kawasumi, A. Usui, Y. Igari, M. Funayama, T. Ueda, T. Ishibashi, H. Saito, Cervical intervertebral separation caused by trauma on post-mortem computed tomography: Possibility of a diagnosis based on intervertebral gas, Forensic Sci. Int. 330 (2022), 111049, https://doi.org/10.1016/j.forsciint.2021.111049.

[10] X. Li, Z. Zeng, Y. Yang, W. Ding, L. Wng, Y. Xu, W. Yang, W. Bi, Warfarin-related epidural hematoma: a case report, J. Int. Med. res. 50(3) (2022) 03000605221082891. 10.1177/03000605221082891.

[11] A. Housni, N. Bankole, A. Ouahabi, Cervical epidural hematoma post-trauma: a case report, Pan Afr. Med. J. 43 (2022) 12. 10.11604/pamj.2022.43.12.28877.

[12] K. Furuya, S. Akiyama, K. Nakamura, Y. Sano, Estimating elapsed time of brain hemorrhage using computed tomography value-based parameters, Nihon Hoshasen Gijutsu Gakkai Zasshi. 68 (7) (2012) 835–840.

[13] G. Inokuchi, D. Yajima, M. Hayakawa, A. Motomura, F. Chiba, Y. Makino, H. Iwase, Is acute subdural hematoma reduced during the agonal stage and postmortem? Int. J. Legal Med. 127 (2013) 263–266, https://doi.org/10.1007/s00414-012-0723-5.

[14] N. Berger, L.C. Ebert, G. Ampanozi, P.M. Flash, D. Gasho, M.J. Thali, T.D. Ruder, Smaller but denser: postmortem changes alter the CT characteristics of subdural hematomas, Forensic Sci. Med. Pathol. 11 (2015) 40–46, https://doi.org/10.1007/s12024-014-9642-8.

[15] J.E. Cavanaugh, A.A. Neath, The Akaike information criterion: Background, derivation, properties, application, interpretation, and refinements, WIREs Comp. Stat. 11 (2019) e1460.

[16] T.W. Arnold, Uninformative parameters and model selection using akaike's information criterion, J. Wildl. Manage. 74 (2010) 1175–1178, https://doi.org/10.1111/j.1937-2817.2010.tb01236.x.

[17] J.M. Kim, Multicollinearity and misleading statistical results, Korean J. Anesthesiol. 72 (2019) 558–569, https://doi.org/10.4097/kja.19087.

[18] K.M. Marcoulides, T. Raykov, Evaluation of variance inflation factors in regression models using latent variable modeling methods, Educ. Psychol. Meas. 79 (2019) 874–882, https://doi.org/10.1177/0013164418817803.

[19] C.E. Metz, Basic principles of ROC analysis, Semin. Nucl. Med. 8 (1978) 283–298, https://doi.org/10.1016/s0001-2998(78)80014-2.

[20] R.H.E. Khouli, K.J. Macura, P.B. Barker, M.R. Habba, M.A. Jacobs, D.A. Bluemke, Relationship of temporal resolution to diagnostic performance for dynamic contrast enhanced MRI of the breast, J. Magn. Reson. Imaging 30 (2009) 999–1004, https://doi.org/10.1002/jmri.21947.

[21] J.N. Mandrekar, Receiver operating characteristic curve in diagnostic test assessment, J. Thorac. Oncol. 5 (2010) 1315–1316, https://doi.org/10.1097/JTO.0b013e3181ec173d.

[22] H. Jamaiyah, A. Geeta, M.N. Safiza, G.L. Khor, N.F. Wong, C.C. Kee, R. Rahmah, A. Z. Ahmad, S. Suzana, W.S. Chen, M. Rajaah, B. Adam, Reliability, technical error of measurements and validity of length and weight measurements for children under two years old in Malaysia, Med. J. Malays. 65 (2010) 131–137.

[23] S.M. Weinberg, N.M. Scott, K. Neiswanger, M.L. Marazita, Intraobserver error associated with measurements of the hand, Am. J. Hum. Biol. 17 (2005) 368–371, https://doi.org/10.1002/ajhb.20129.

[24] T. Fujimiya, Legal medicine and the death inquiry system in Japan: A comparative study, Legal Med. 11 (2009) S6–S8, https://doi.org/10.1016/j.legalmed.2009.02.022.

[25] P.M. Leth, The use of CT scanning in forensic autopsy, Forensic Sci. Med. Pathol. 3 (2007) 65–69, https://doi.org/10.1385/FSMP:3:1:65.

[26] S. Shiotani, M. Shiigai, Y. Ueno, N. Sakamoto, S. Atake, M. Kohono, M. Suzuki, H. Kimura, K. Kikuchi, H. Hayakawa, Postmortem computed tomography findings as evidence of traffic accident-related fatal injury, Radiat. Med. 26 (2008) 253–260, https://doi.org/10.1007/s11604-007-0223-6.
[27] T. Okuda, S. Shiotani, N. Sakamoto, T. Kobayashi, Background and current status of postmortem imaging in Japan: Short history of "Autopsy imaging (Ai)", Forensic Sci. Int. 2 (2013) 3–8, https://doi.org/10.1016/j.forsciint.2012.03.010.
[28] A. Christe, P. Flach, S. Ross, D. Spendlove, S. Bolliger, P. Vock, M.J. Thali, Clinical radiology and postmortem imaging (Virtopsy) are not the same: Specific and unspecific postmortem signs, Legal Med. 12 (2010) 215–222, https://doi.org/10.1016/j.legalmed.2010.05.005.
[29] F. Bolster, Z. Ali, B. Daly, The "pseudo-CT myelogram sign": an aid to the diagnosis of underlying brain stem and spinal cord trauma in the presence of major craniocervical region injury on post-mortem CT, Clin. Radiol. 72 (1085) (2017) e11–1085.e15, https://doi.org/10.1016/j.crad.2017.07.019.
[30] K. Carpenter, T. Decater, J. Iwanaga, C.M. Maulucci, C.J. Bui, A.S. Dumont, R. S. Tubbs, Revisiting the vertebral venous plexus-a comprehensive review of the literature, World Neurosurg. 145 (2021) 381–395, https://doi.org/10.1016/j.wneu.2020.10.004.
[31] R.J.M. Groen, H.J. Groenewegen, H.A. van Alphen, P.V. Hoogland, Morphology of the human internal vertebral venous plexus: A cadaver study after intravenous araldite CY 221 injection, Anat. Rec. 249 (1997) 285–294, https://doi.org/10.1002/(SICI)1097-0185(199710)249:2<285::AID-AR16>3.0.CO;2-K.
[32] E. Wnuk, E. Maj, T. Dziedzic, A.P. Piętowska, Spinal Epidural Venous Plexus Enlargement as a Cause of Neurologic Symptoms: Vascular Anatomy and MRI Findings, Neuro India. 68 (2020) 1238–1241, https://doi.org/10.4103/0028-3886.294546.
[33] A. Whiting, J. Ciancarelli, J. Germano, A. Mysterious Bleed, A Case of Spontaneous Spinal Epidural Hematoma After Atrial Fibrillation Ablation, JACC: Case Rep. 13 (2023), 101817, https://doi.org/10.1016/j.jaccas.2023.101817.
[34] C.A. Given, J.H. Burdette, A.D. Elster, D.W. Williams, Pseudo-subarachnoid hemorrhage: a potential imaging pitfall associated with diffuse cerebral edema, AJNR, Am. J. Neuroradiol. 23 (2003) 254–256.
[35] N. Takahashi, C. Satou, T. Higuchi, M. Shiotani, H. Maeda, T. Hirose. Quantitative analysis of intracranial hypostasis: comparison of early postmortem and antemortem CT findings, AJR. Am. J .Roentgenol. 195 (2010) W388-W393. 10.2214/AJR.10.4442.
[36] G. Shirota, W. Gonoi, M. Ikemura, M. Ishida, Y. Shintani, H. Abe, M. Fukayama, T. Higashida, H. Okuma, O. Abe, The pseudo-SAH sign: an imaging pitfall in postmortem computed tomography, Int. J. Legal Med. 131 (2017) 1647–1653, https://doi.org/10.1007/s00414-017-1651-1.
[37] A. Platt, J. Collins, E. Ramos, F.D. Goldenberg, Pseudosubarachnoid hemorrhage: A systematic review of causes, diagnostic modalities, and outcomes in patients who present with pseudosubarachnoid hemorrhage, Surg. Neurol. Int. 12 (2021) 29. 10.25259/SNI_905_2020.
[38] M.E. Fretwell, N. Mullaguri, S. Sivakumar, M. Knipfing, Pseudo Subarachnoid Hemorrhage Sign in Bacterial Meningitis in a Patient Presenting With Acute Ischemic Stroke: A Novel Radiological Clue to Rapid Diagnosis, Cureus. 14 (2022) e25283.
[39] M.A. Baig, L.J. Pedro, A. Gebreyohanes, A. Vastani, M. China, D. Kalaitzoglou, J. Bartram, H. Eid, C. Bleil, D. Bell, N. Thomas, I. Malik, G. Grahovac, Prognostic factors for surgically managed spontaneous spinal epidural hematoma: a single-center case series of 18 patients, Operative, Neurosurgery. 24 (2023) 391–403, https://doi.org/10.1227/ons.0000000000000562.
[40] F.C. Tamburrelli, M.C. Meluzio, G. Masci, A. Perna, A. Burrofato, L. Proietti, Etiopathogenesis of Traumatic Spinal Epidural Hematoma, Neurospine 15 (1) (2018) 101–107.
[41] T. Noguchi, S. Oguri, T. Yamaguchi, T. Kamitani, M. Saku, M. Kimura, Y. Nakamura, J. Murakami, S. Nagata, S. Nagano, J. Furuya, Spinal epidural hematoma: relationship between imaging findings and neurological outcomes, Nihon Igaku Hoshasen Gakkai Zasshi. 63 (2003) 385–389.

論文目録

I　　主論文

Distinguishing true from pseudo hematoma in the cervical spinal canal using postmortem computed tomography.

Kuninaka, H., Usumoto, Y., Tanabe, M., Ogawa, N., Mukai, M., Nasu, A., Maeda, K. , Fuke, C.,　Sawamura, S., Yamashiro, T., Utsunomiya, D., and Ihama Y.：
雑誌名：Legal Medicine（Tokyo）Vol.48, 101821, 2023

II　　副論文なし

III　　参考論文

1　Identification of aortic injury site using postmortem non–contrast computed tomography in road traffic accident.
Horie, K., Ihama, Y., Aso, S., Kuninaka, H., Mochizuki, H., Tamashiro. T., Kato, S., and Utsunomiya, D.：
雑誌名：Radiol Case Rep（USA）Vol. 16(1), p5-8, 021

2　Kinetics and distribution of benzalkonium compounds with different alkyl chain length following intravenous administration in rats.
Kera, H., Fuke, C., Usumoto, Y., Nasu, A., Maeda, K., Mukai, M., Sato, W., Tanabe, M., Kuninaka, H., and Ihama Y.：
雑誌名：Legal Medicine（Tokyo）Vol.48, 101821, 2021

3　リアルタイム RT-PCR 法により体液や臓器から新型コロナウイルスを検出した一例
田邊桃佳，前田一輔，解良仁美，國中光，佐藤若菜，向井萌，那須亜矢子，臼元洋介，福家千昭，井濱容子：
雑誌名：法医病理 第 27 巻第 1 号 75 頁～77 頁 2021 年

4　ベビーチェアのシートベルトの不適切な装着により死亡した幼児の 1 例
田邊桃佳，臼元洋介，國中光，解良仁美，佐藤若菜，向井萌，那須亜矢子，前田一輔，福家千昭，井濱容子：
雑誌名：法医学の実際と研究 第 64 巻 107 頁～111 頁 2021 年